Reference: *Biol. Bull.* **193:** 125–140. (October, 1997)

Nuclear Microprobe Mapping of Statoliths of Chokka Squid *Loligo vulgaris reynaudii* d'Orbigny, 1845

M. D. DURHOLTZ[1], M. R. LIPINSKI[2,*], W. J. PRZYBYLOWICZ[3,†], AND J. MESJASZ-PRZYBYLOWICZ[3]

[1] *Department of Zoology, University of Cape Town, Rondebosch, 7700, South Africa;* [2] *Sea Fisheries Research Institute, Private Bag X2, Roggebaai 8012, South Africa; and* [3] *Van de Graaff Group, National Accelerator Centre, P.O. Box 72, Faure 7131, South Africa*

Abstract. Loliginid squid statoliths were broken in half and their elemental composition was assessed using the nuclear microprobe technique. Proton induced X-ray emission and proton backscattering were used simultaneously. True, quantitative maps of calcium and strontium distribution in the frontal plane were obtained using a rapid-matrix-transform method called Dynamic Analysis. These measurements were complemented by observations with scanning electron microscopy and light microscopy. In juvenile and adult statoliths, Sr was concentrated in the wing and adjacent areas, whereas the Ca concentration was highest on the edge of the lateral dome. In contrast, Sr and Ca were uniformly distributed in the statoliths of paralarval squid. Increments showed best definition in the areas anterior and adjacent to the wing, corresponding to areas of high Sr content. Although temperature, sex, maturity, and the administration of oxytetracycline may influence the quantitative distribution of Ca and Sr in the statoliths of adult squid, they do not appear to affect the general pattern described above. The finding that Sr is concentrated in regions adjacent to the macula where the clearest increments are found in loliginid statoliths supports the hypothesis linking strontium with the regulation of statolith deposition and the definition of daily increments.

Received 22 January 1997; accepted 23 June 1997.

* Author to whom correspondence should be addressed; e-mail: lipinski@sfri.wcape.gov.za.

† On leave from the Faculty of Physics and Nuclear Techniques, Academy of Mining and Metallurgy, 30-059 Cracow, Poland.

Introduction

Considerable interest has been directed at the use of statoliths to estimate the age of squid. However, as with determining the age of fish from their otoliths, several unresolved problems complicate the estimates derived from the analysis of statolith microstructure. At present, very subjective criteria are applied to distinguish daily increments from other potentially confusing microstructural features such as sub-daily rings and checks. This element of subjectivity is probably the primary cause of the highly variable age estimates reported for some species of squid (Villanueva, 1992, vs. Lipinski *et al.*, 1993; Natsukari *et al.*, 1993, vs. Arkhipkin *et al.*, 1996). The interpretation of such features has been simplified through an understanding of the physiology of their underlying causal mechanisms (Gauldie *et al.*, 1995). In their paper on modeling of otolith growth, Romanek and Gauldie (1996) stated: "Theoretical models of otolith growth would greatly assist in establishing criteria for the validation of age marks, but they are surprisingly uncommon given the extent of disagreement between age estimation techniques." Research towards this goal is relatively well advanced for fish otoliths (Gauldie and Nelson, 1990; Gauldie *et al.*, 1995; Romanek and Gauldie, 1996), but apart from the studies of Morris (1988) and Lipinski (1986, 1993), very little attention has been directed to the physiological mechanisms by which squid form statoliths.

We feel that there are not enough basic data on the elemental composition and dynamics of various components of the vestibular systems of fish and squid (*e.g.*,

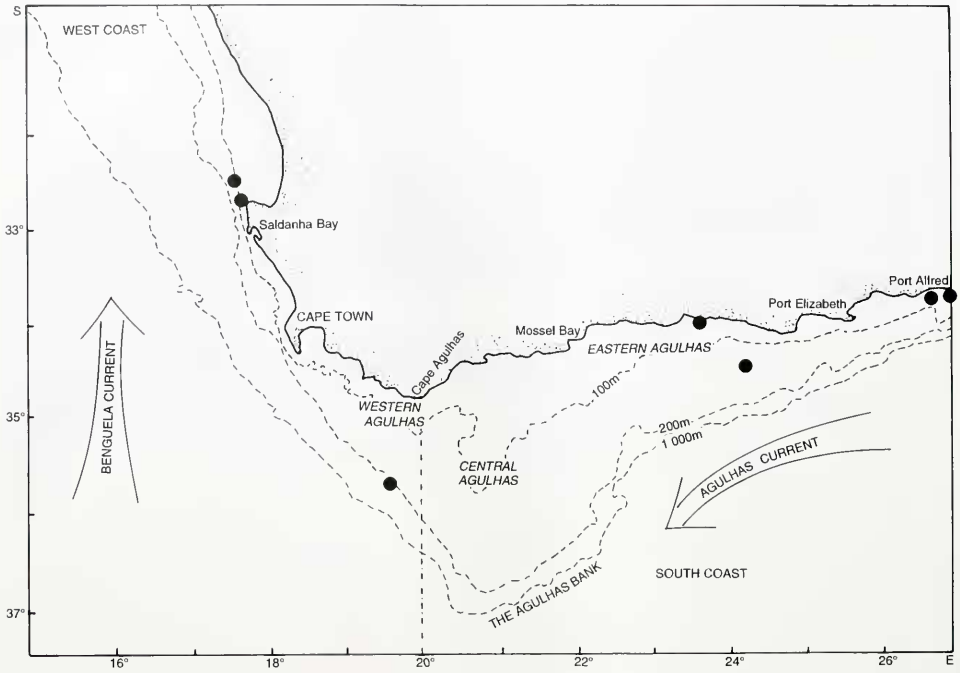

Figure 1. Distribution of squid sampling sites.

otoliths/statoliths, endolymph fluid, maculae) to improve the existing models. Data on statolith deposition are particularly important, as emphasized by Romanek and Gauldie (1996). An understanding of this process could provide valuable insights into the nature and operation of the circadian rhythm presumed to be implicit in the deposition of daily increments, as well as clarifying the structural and functional characteristics of the increments. This latter aspect is felt to be of crucial importance in the application of the statolith-based aging technique. Our understanding of these characteristics in fish otoliths has been greatly furthered by investigations of the elemental composition of otoliths. For example, Gauldie *et al.* (1992, 1995) used a proton microprobe to evaluate otolith age estimates of two fish species by comparing patterns of checks, cycles in increment width, and cycles in strontium and calcium composition. Mugiya and Satoh (1995) were able to analyze calcium and strontium levels within increments by using X-ray microanalysis. Unfortunately, the goal of the latter study cannot be realized in loliginid squid because the increment widths in the statoliths are typically on the order of 1 μm or less, below the resolution limits of current microanalytical techniques. However, as has been demonstrated by Gauldie *et al.* (1992, 1995), microanalysis of elemental composition on a larger scale than that of increments can generate valuable information about the deposition of otoliths and statoliths, and thus may help answer questions about the formation of increments.

In the current work we sought (1) to detect any qualitative associations between statolith microstructure (specifically increment appearance) and the distribution of calcium and strontium within squid statoliths, and (2) to assess whether any patterns discovered were consistent between sexes, stages of development, and ambient temperatures. We also considered the influence of oxytetracycline (OTC) marking on the elemental composition of statoliths. Results of validation experiments employing this substance as a chemical marker indicated that its incorporation into the statoliths may have been associated with some physiological stress, and hence may have had some influence on the crystals deposited while the

Table I

Description of material used in the PIXE analysis

Type of material	*n*	ML (mm)	Capture date	Location	Sex and maturity*
paralarvae	4	<2	10/10/91	Kromme Bay	
juveniles	2	65	15/09/92	Plettenberg Bay	M I
		78	15/09/92	Plettenberg Bay	M I
adults	6	154	15/09/92	Plettenberg Bay	M III
(mixed material)		175	11/11/93	Kromme Bay	F III
		198	16/09/92	S. of TCNP	M III
		250	05/01/94	Agulhas Bank	M II
		263	12/11/93	Kromme Bay	M V
		350	11/11/93	Kromme Bay	M V
adults	5	171	01/03/93	aquarium†	F III
(OTC marked)		182	14/11/93	aquarium†	M IV
		200	01/03/93	aquarium†	M III
		240	22/12/93	aquarium†	M V
		324	15/11/93	Kromme Bay	M V
adults	3	182	20/09/92	Port Alfred	F V
(warm water)		214	20/09/92	Port Alfred	M III
		268	20/09/92	Port Alfred	M V
adults	3	179	13/01/94	St. Helena Bay	F II
(cold water)		202	13/01/94	St. Helena Bay	M II
		225	13/01/94	St. Helena Bay	M III

* M—male, F—female; maturity stages (I–VI) assessed according to the scale of Lipinski and Underhill (1995).

† Aquarium maintenance material was all captured in False Bay.

OTC was being metabolized (Lipinski *et al.*, unpub. data).

Strontium concentrations in biogenic calcium carbonates are often a limiting factor in studies of this nature. The proton microprobe system is able to measure elements at levels approaching a few parts per million, with the further advantage of a data acquisition system that permits quantitative mapping with full-spectrum processing at every pixel in the image.

Materials and Methods

Statolith collection and preparation

Statoliths of chokka squid (*Loligo vulgaris reynaudii*) were collected during several summer cruises of RS *Africana*, RS *Algoa*, and various commercial vessels in the years 1992–1994. The area of collection (Fig. 1) extended from St. Helena Bay on the west coast of South Africa to Port Alfred on the southeast coast. The list of collected material is given in Table I. The three warm-water squid were collected at 30-m depths at sites near Port Alfred influenced by the warm Agulhas Current. The bottom temperature at these sites was 17.6°C at the time of collection. In contrast, the three cold-water squid were collected in cold upwelled water near St. Helena Bay at depths of 100 m; the bottom temperature at these sites was 9.1°C at the time of collection. The OTC-marked statoliths were obtained from laboratory validation studies in which up to 0.1 ml of an OTC solution (Lipinski, 1986) was injected into the ventral mantle musculature of squid to mark the statoliths with a fluorescent label. After marking, the squid were maintained for periods ranging from 2 to 30 days in aquaria supplied with a continuous flow of fresh seawater and exposed to the ambient light regime. The squid were fed a diet of live fish *ad libitum* for the duration of the experiments.

Statoliths were dissected according to the method of

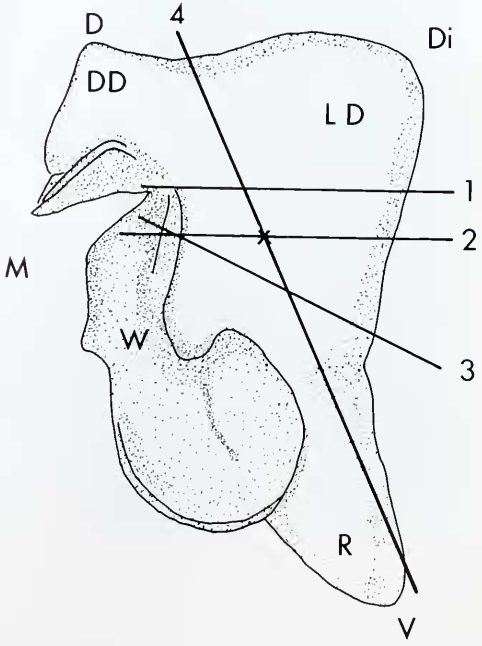

Figure 2. Diagram illustrating an anterior view of the statolith from the left statocyst of a chokka squid, showing the orientation and parts of squid statoliths, as well as the break and section planes used in this study. D—dorsal, V—ventral, M—medial, Di—distal (lateral), DD—dorsal dome, LD—lateral dome, R—rostrum, W—wing, 1—frontal break above the nucleus (the position of the nucleus is indicated with an 'x'), 2—frontal break through the nucleus, 3—oblique frontal break below the nucleus, 4—sagittal section through the nucleus.

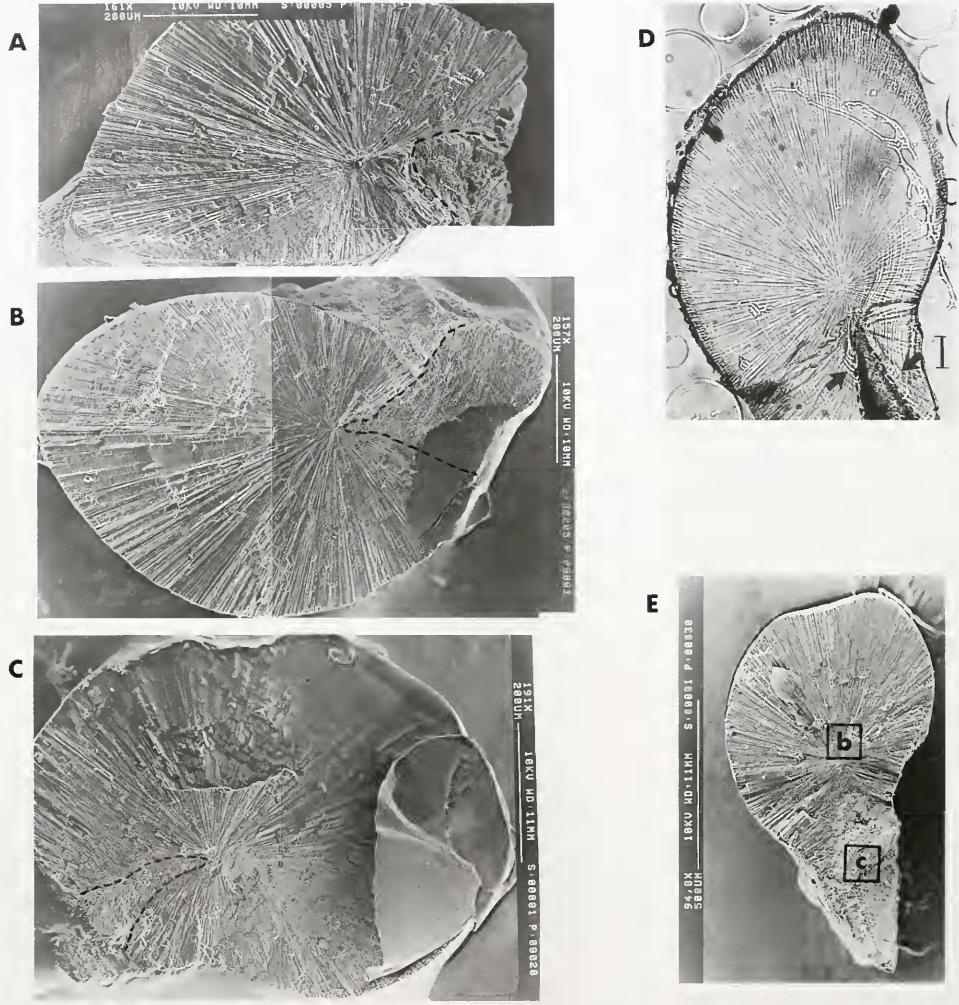

Figure 3. Internal structure of chokka statoliths; the inclusion of wing crystals is outlined with a dotted line. (A) Scanning electron micrograph (SEM) of statolith (ML = 175 mm; ♀V) broken below the nucleus (plane 3 in Fig. 2). (B) SEM of statolith (ML = 268 mm; ♂V) broken at the level of the nucleus (plane 2 in Fig. 2). (C) SEM of statolith (ML = 179 mm; ♀II) broken above the nucleus (plane 1 in Fig. 2). (D) Light micrograph of ground and polished frontal section of a chokka statolith (ML = 57 mm; juvenile) showing the wing and position of clearest increments (arrows); the scale bar is 50 μm. (E) SEM of statolith (ML = 324 mm; ♂V) illustrating the position of the microprobe maps presented in Fig. 6B, C.

Lipinski (1981) and stored dry in small plastic tubes. They were fractured in the frontal plane using a clean and sterilized scalpel blade. The line of the break was determined by the approximate position of the nucleus and varied relatively little (Fig. 2). Ten statoliths, however, were broken below the nucleus where the rostrum

forms an angle with the lateral dome (plane 3 in Fig. 2), and ten statoliths were broken above the nucleus (plane 1 in Fig. 2). The surface of the break was then viewed under a stereomicroscope, and only statoliths with relatively clean and even surfaces were accepted for further preparation. The statolith halves were mounted on a Formvar membrane spread on a thin aluminum frame using Araldite Rapid glue. A second frame with Formvar was glued on top of the statolith's frontal surface and coated with a thin layer of carbon. Once the nuclear microprobe observations had been completed, the samples were re-mounted on aluminum stubs, re-coated with carbon, and viewed under a Stereoscan 200 scanning electron microscope (SEM). To locate areas of the most prominent increments, statoliths were prepared according to Lipinski and Durholtz (1994) and viewed and photographed under a Zeiss light microscope. Terminology used is after Clarke (1978) and Lipinski *et al.* (1991).

Microprobe measurements

The selection of the microanalytical technique for this study was based on two criteria, namely lateral resolution and sensitivity. Ideally, a technique with a lateral resolution of about 0.5 μm or less (the spatial scale of increments in squid statoliths), with a sensitivity permitting quantitative mapping of the elements of interest, is required. Since Sr concentration was of particular interest in this study, the analytical technique had to be capable of measuring this element at levels approaching a few parts per million. Although the proton microprobe is capable of this level of sensitivity, it cannot fulfill the criterion for lateral resolution. Techniques that provide such high levels of resolution (such as electron microprobes in energy dispersed spectrometry mode, or electron energy loss spectroscopy) require very thin samples; these are almost impossible to obtain from squid statoliths, which tend to disintegrate when very fine sectioning is attempted. Furthermore, it is doubtful whether such techniques are suitably sensitive for Sr analysis. To our knowledge, no technique currently satisfies both the lateral resolution and sensitivity requirements of this study. The use of the proton microprobe consequently represents a compromise between these two criteria.

The analyses were performed with 3.0 MeV protons, using the nuclear microprobe of the National Accelerator Centre (NAC). The details of the experimental setup have been reported previously (Tapper *et al.*, 1993, Prozesky *et al.*, 1995). Two complementary techniques, proton induced X-ray emission (PIXE) and proton back scattering (BS) were used simultaneously. The beam spot size was about 3 μm $\times$ 3 μm for proton currents of 200–400 pA. The proton currents were maintained within this range

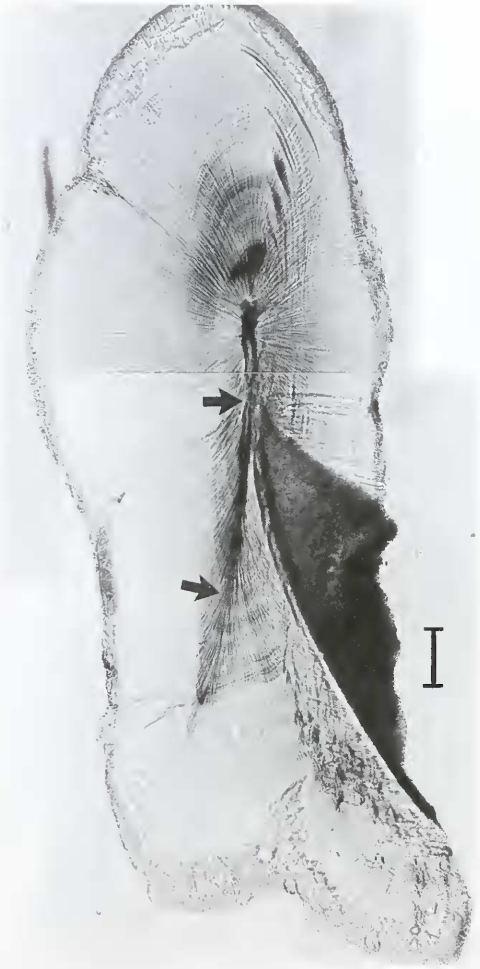

Figure 4. Light micrograph of a ground and polished sagittal section of a statolith (ML = 320 mm; ♂V) showing the transverse axis of crystallization (arrows). The scale bar is 100 μm.

because higher currents destroyed the Formvar layer mounted on top of the statolith's frontal surface, affecting the charge collection.

PIXE spectra were registered using a Si(Li) X-ray detector, situated about 37 mm away from the target at 135° to the incoming beam direction and separated from the evacuated specimen chamber by means of an intervening

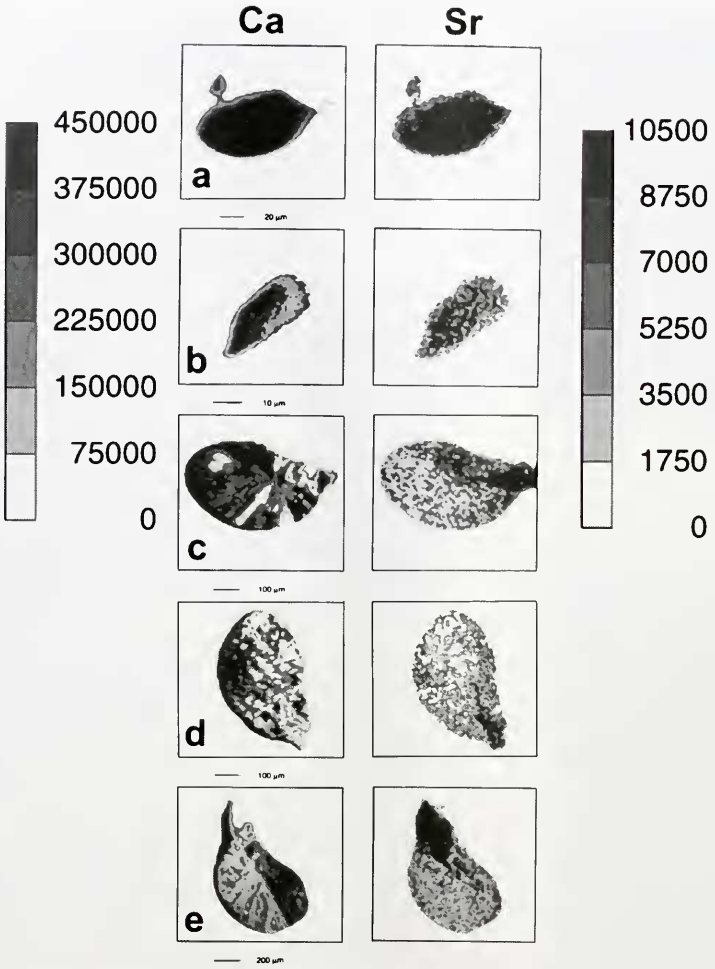

Figure 5. Ontogenetic changes in calcium and strontium concentrations in the squid statolith (values in ppm): (a) paralarva; (b) paralarva; (c) ML = 65 mm, ♂I; (d) ML = 78 mm, ♂I; (e) ML = 214 mm, ♂III.

25-μm Mylar window. An additional 40-μm Al absorber was used to reduce the intensity of Ca K X-ray lines and allowed the simultaneous measurements of Ca as well as of minor and trace elements. The setup was calibrated using thick pure elements and glass standards as well as thin standards from Micromatter (Prozesky *et al.*, 1995; van Achterbergh *et al.*, 1995). PIXE spectra were analyzed using the GeoPIXE suite of programs (Ryan *et al.*, 1990; Ryan and Jamieson, 1993). This package allows the analysis of X-ray spectra with complete corrections for beam stopping, X-ray attenuation, and secondary fluorescence of thick targets.

Backscattered protons were registered with an annular Si surface barrier detector, situated at 176° to the incom-

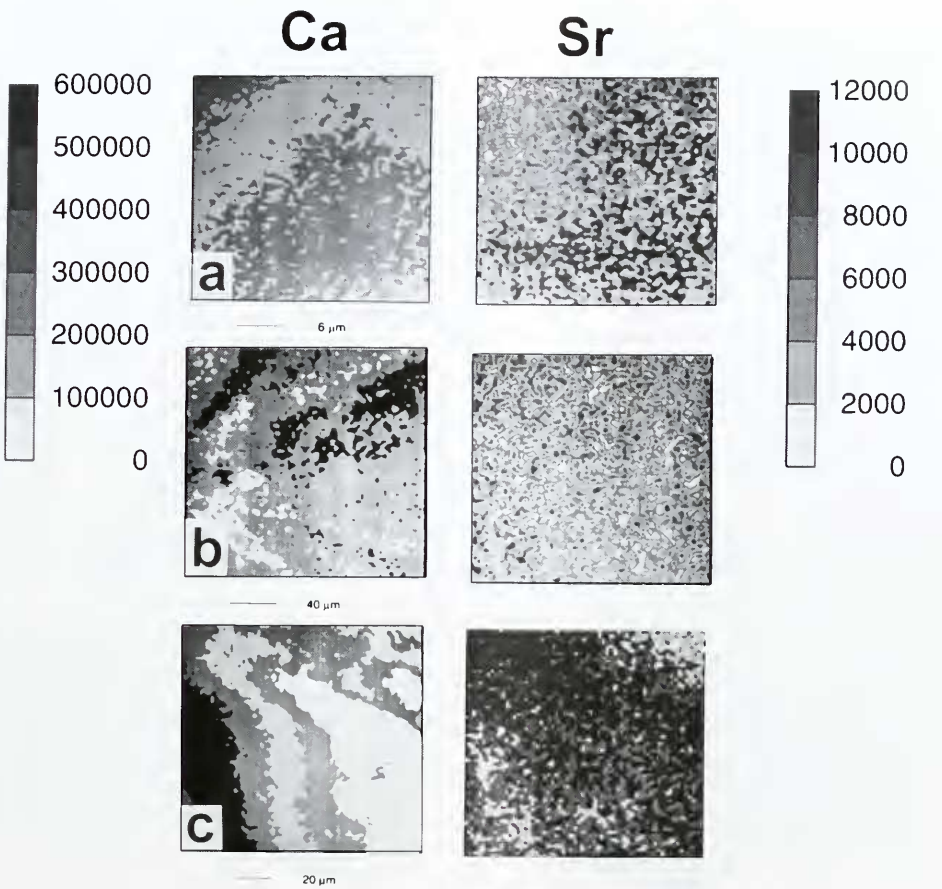

Figure 6. Ontogenetic and structural changes in calcium and strontium concentrations (values in ppm) in selected structures of squid statoliths: (a) paralarva, nucleus area; (b) adult (ML = 324 mm, ♂V), nucleus area (see Fig. 3E); (c) adult (same individual as b, see Fig. 3E), wing area.

ing beam direction. The simulations of proton BS spectra were performed with a modified version of RUMP, a software package that performs the simulations of Rutherford backscattering spectra (Doolittle, 1986), using experimental cross-sections for isotopically natural C and O at a laboratory angle of 170° (Amirikas *et al.*, 1993). No correction was made for this slight difference in angle between the experimental and simulated geometry.

Elemental maps were made using a recently developed rapid matrix transform method called Dynamic Analysis (DA) (Ryan and Jamieson, 1993; Ryan *et al.*, 1995). This is a part of the GeoPIXE package and allows for the production of true elemental images. The images are inherently overlap-resolved and background-subtracted, and the maps are generated on-line. Final maps give quantitative elemental images and the intensity is given in parts per million.

Mapping was performed systematically. First one or more point analyses were made in selected regions of the statolith to find a representative PIXE spectrum with all

Table II

Calcium and strontium composition of squid statoliths

Statolith	Element	Concentration (ppm) mean	Concentration (ppm) SD	Sr/Ca (%)
paralarvae	Ca	3.763×10^5	5.304×10^4	2.25
	Sr	8.451×10^3	157	
	Ca	3.374×10^5	4.779×10^4	2.34
	Sr	7.892×10^3	164	
	Ca	3.266×10^5	4.550×10^4	3.03
	Sr	9.906×10^3	231	
	Ca	3.468×10^5	4.894×10^4	2.20
	Sr	7.614×10^3	143	
ML 324 mm (OTC*) (lateral dome)	Ca	4.415×10^5	6.230×10^4	1.88
	Sr	8.321×10^3	149	
ML 324 mm (OTC*) (wing)	Ca	3.461×10^5	4.789×10^4	3.39
	Sr	1.174×10^4	206	

* Statoliths that were labeled with oxytetracycline.

elements present and to evaluate the specimen thickness for proper matrix corrections. It was found that the specimens were infinitely thick for microanalytical purposes (*i.e.,* their thickness exceeded the depth of penetration of the proton beam), and approximation of the sample composition as $CaCO_3$ was sufficient for matrix correction. The influence of the Formvar layer on top of specimens (about 0.5 μm thick) was found to be negligible, and the correction for this layer was not included.

Scan size was selected according to the size of individual specimens. Scanned regions were divided into 64 × 64 pixels. The Interactive Data Language (IDL) software package (Research Systems, Inc., 1993) was used for data presentation, and the maps are contours linking pixels with similar values.

Statistical analysis of the influence of temperature

As a preliminary investigation of the possible influence of temperature on calcium and strontium levels in squid statoliths, the data from three individuals of similar size and maturity from each of the two temperature regimes were compared. Raw data files obtained from the microprobe analyses provided measurements of calcium and strontium concentration within each pixel of the maps. To ensure that the data were representative of the temperature regime at which the squid were captured, analysis was restricted to points around the periphery of the lateral dome (*i.e.,* the most recently deposited mineral). Concentrations of both calcium and strontium were obtained for each pixel around the periphery, Sr/Ca ratios were calculated for each pixel, and the data were subjected to an analysis of variance (ANOVA) to test for differences between the statoliths and between the temperature regimes. STATISTICA, a commercially available software package, was used for all statistical procedures.

Results

Morphology of the surface of the statolith frontal break

SEM observations of the surfaces of the frontal breaks (indicated in Fig. 2) showed aragonite crystals radiating outwards from a central point (Fig. 3). In the breaks through the nucleus (plane 2 in Fig. 2), this central point is clearly the focus. However, in breaks above and below the nucleus (planes 1 and 3 in Fig. 2), the central point is not the focus, suggesting that a previously undescribed axis of crystallization extends dorsoventrally from the focus. LM observations of ground and polished sagittal sections (plane 4 in Fig. 2) through the focus clearly show the axis extending ventrally from the focus beyond the nucleus and possibly the protostatolith, into the rostrum (Fig. 4). The dorsal component of the axis above the focus is not clearly apparent, and probably does not extend very far, if at all, beyond the nucleus.

The breaks differed, however, with respect to the medial inclusion of the irregularly orientated wing crystals into the lateral dome. In the planes above and below the focus, the inclusion of wing crystals does not reach the axis of crystallization (Fig. 3A, C). In contrast, when a statolith is broken through the focus, the triangular wing inclusion clearly originates at the focus. LM observations of the frontal break in the same plane as the nucleus showed that the clearest increments were located in the regions adjacent and anterior to the triangular inclusion of wing crystals (Fig. 3D).

Maps of Ca and Sr distribution in loliginid statoliths: ontogenetic changes

In chokka hatchlings, Ca and Sr seem to concentrate in the middle of the statolith, but this may be an artifact related to the thickness of the sample (see Materials and Methods). It is more likely that these elements are distributed uniformly through the break. Sr levels were considerably higher than those measured in the lateral domes of older squid, but were either comparable to levels in the wings of both juvenile and adult squid, or intermediate (Figs. 5 and 6; Table II).

In juveniles and adults of mantle lengths 65 mm and larger, patterns of Ca and Sr were generally very similar among individuals. The distribution of Sr showed the

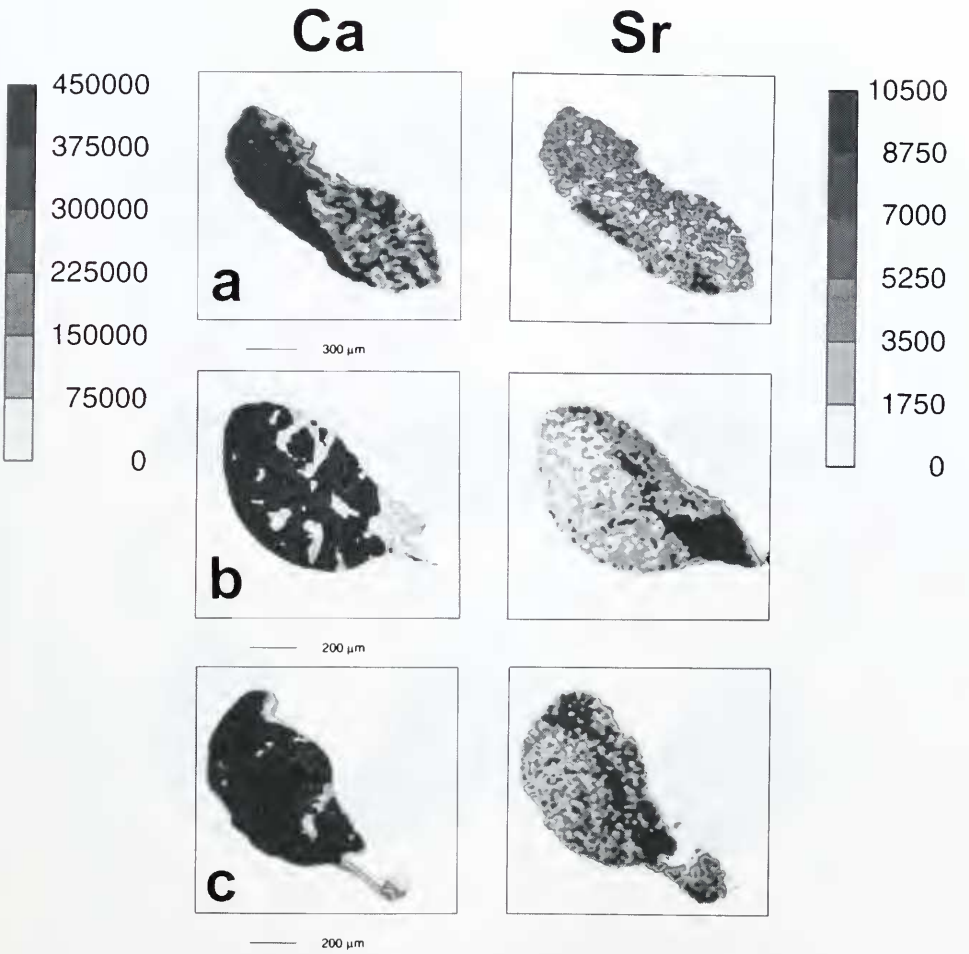

Figure 7. Calcium and strontium concentrations (values in ppm) in transverse sections of the squid statolith at levels: (a) below the nucleus (ML = 175 mm, ♀V); (b) at the nucleus (ML = 182 mm, ♂IV, OTC marked squid, 19 days post-marking); (c) above the nucleus (ML = 179 mm, ♀II).

most striking and consistent pattern. In all planes investigated, Sr exhibited uniformly high concentrations in the wing crystals (Figs. 5, 7, 9) and adjacent areas, with patches of high Sr concentration extending along a curving axis into the anterior regions of the lateral dome. Ca distribution patterns were less clearly defined, showing great variability among individuals. In general however, Ca concentrations were higher in the lateral domes (particularly in the peripheral regions) and lower in the wing area (Fig. 5, 7, 8).

Effects of temperature, sex, and oxytetracycline injection

Although the maps of statoliths collected in warm and cold water showed a great deal of variability, the general

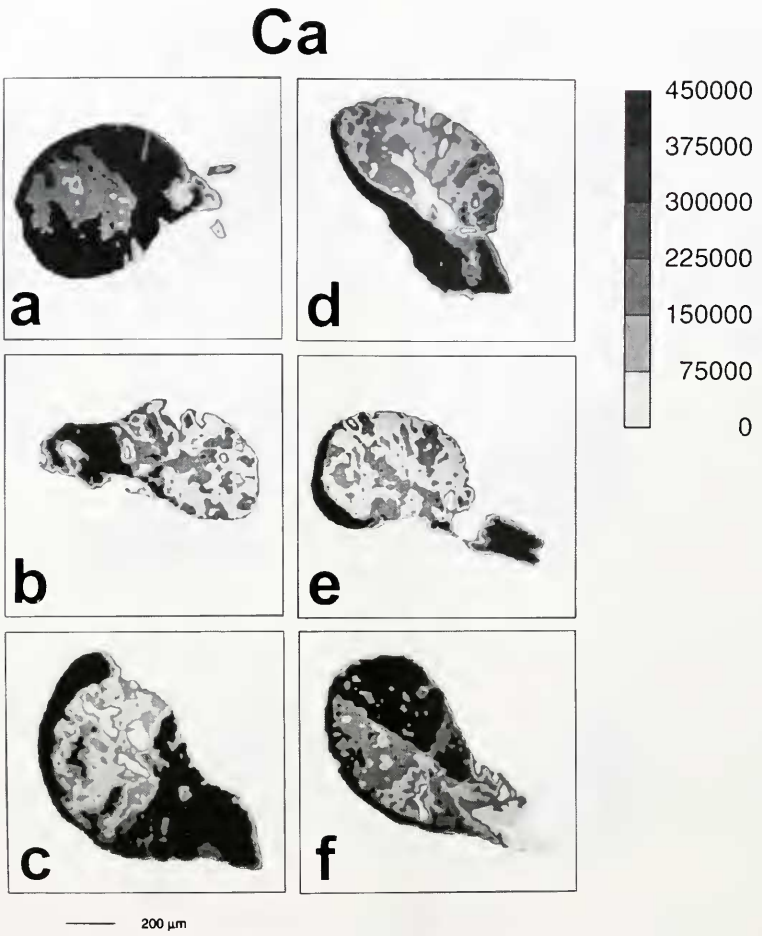

Figure 8. Calcium concentrations (values in ppm) in statoliths from cold waters (a–c) and warm waters (d–f). (a) ML = 179, ♀II; (b) ML = 202 mm, ♂II; (c) ML = 225 mm, ♂III; (d) ML = 182 mm, ♀V; (e) ML = 214 mm, ♂III; (f) ML = 268 mm, ♂V.

structural patterns described above did not appear to differ between the two temperature regimes (Figs. 8 and 9). Whereas mean calcium concentrations around the periphery of the lateral domes were significantly different between the two temperatures (Table III), with mean calcium concentrations slightly higher in cold-water statoliths than in warm-water statoliths, no difference was found in mean strontium concentrations. Corresponding Sr/Ca ratios showed significant differences with temperature: ratios were higher in warm-water statoliths than in those from cold waters (Table III). Although the variation in calcium concentrations and Sr/Ca ratios between the two temperature groups was statistically significant, variation in these variables, as well as in the strontium concentrations, was found to be significant among the statoliths within each temperature group (Table IV). *A posteriori* Tukey multiple comparison tests indicated that the differences in calcium, strontium, and Sr/Ca levels among the

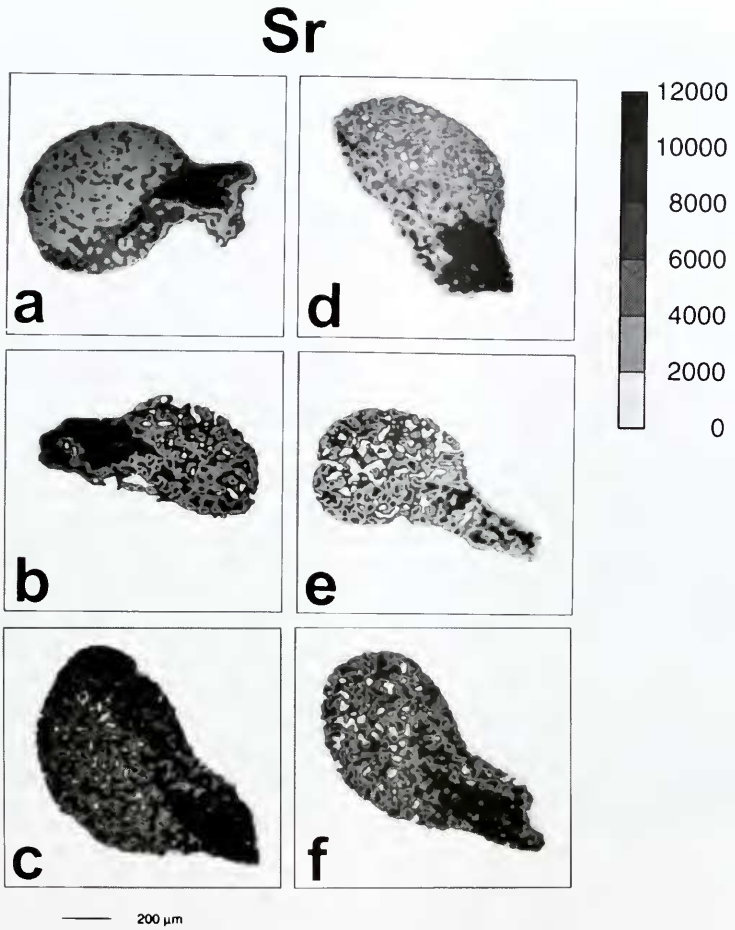

Figure 9. Strontium concentrations (values in ppm) in statoliths from cold waters (a–c) and warm waters (d–f). Same individuals as in Fig. 8.

various statoliths had no clear pattern that could possibly be attributed to a temperature effect (Table V).

No consistent sex- and maturity-related differences were detected (Figs. 7 and 8). OTC incorporation into the statolith had no apparent effect on the structural patterns observed (Fig. 7B vs. Figs. 8, 9).

Other elements present

In addition to Ca and Sr, the elements detected by PIXE were Cr, Fe, Zn, Cu, and Br. Cr and Fe, which were confined to the extreme borders of the specimens, with very low concentrations within the body of the statolith, were judged to be experimental artifacts introduced during the preparation process rather than genuine components of the statoliths. The remaining elements (Zn, Cu, and Br) were present in only some of the statoliths (Figs. 10 and 11), but when present, their distribution suggested that they were not impurities. The distribution of these elements cannot be deduced from these limited data, but a more detailed discussion of the distri-

Table III

Comparisons of mean calcium concentrations (ppm), mean strontium concentrations (ppm) and Sr/Ca ratios between warm- and cold-water statoliths

Statolith type	Calcium				Strontium				Sr/Ca			
	Mean	SD	*n*	ANOVA*	Mean	SD	*n*	ANOVA*	Mean	SD	*n*	ANOVA*
Warm-water	247,378	52,606	394	$F = 76.497$	5210	1212	394	$F = 3.779$	0.0221	0.0075	394	$F = 14.114$
Cold-water	281,161	57,518	419	$P < 0.001$	5370	1131	419	$P = 0.052$	0.0201	0.0074	419	$P < 0.001$

* ANOVA conducted on data pooled over all statoliths in each temperature group.

bution of these elements can be found in Lipinski *et al.*, (in press).

Discussion

Morphology

Interpretation of previously reported data on statolith structure (Lipinski *et al.*, 1991; Lipinski, 1991, 1993) suggests a single nucleation site, with calcification radiating from that site. We propose an alternative, namely that further calcification proceeds along an axis extending dorsoventrally from the focus. Further research should be directed at this axis—specifically at the potential complications in interpreting increment patterns and increment counts.

Maps: ontogenetic changes of Ca and Sr content

The ontogenetic changes we have described in Ca and Sr distribution patterns in the statoliths of *Loligo vulgaris reynaudii* provide information concerning the deposition of squid statoliths. We interpret the patterns observed in paralarval statoliths as showing uniformly high concentrations of Ca and Sr. With continuing growth of the animal, and deposition of statolith layers, there is a shift to increasing Ca concentration in peripheral areas of the statolith (especially posterior), distant from the wing area. Sr, on the other hand, shows consistently high concentrations in the wing crystals themselves, in areas adjacent and anterior to the wing, and in the anterior regions of the lateral dome.

These observations are consistent with the hypothesis of biomineralization in the squid statocyst proposed by Lipinski (1993), namely that Sr is secreted into the endolymph from the cells of the macula, whereas Ca is supplied from sites distant to the macula as suggested by Morris (1988). With the onset of deposition in squid embryos, Sr precipitation occurs at the macula (reactions according to Lipinski, 1993), accounting for the high Sr concentrations in paralarval statoliths. As deposition progresses and the statolith increases in size, deposition sites on the posterior and lateral areas of the statolith become increasingly distant from the Sr supply in the macula, hence Sr concentrations are low in these areas.

Table IV

Comparisons of mean calcium concentrations (ppm), mean strontium concentrations (ppm) and Sr/Ca ratios between warm- and cold-water statoliths

Statolith*	Calcium				Strontium				Sr/Ca			
	Mean	SD	*n*	ANOVA	Mean	SD	*n*	ANOVA	Mean	SD	*n*	ANOVA
Warm-water												
W1 (268 mm)	267,247	52,294	123		5207	1337	123		0.0200	0.0059	123	
W2 (182 mm)	229,668	63,690	138	$F = 17.916$	5430	1277	138	$F = 4.286$	0.0256	0.0098	138	$F = 25.817$
W3 (214 mm)	247,361	33,452	158	$P < 0.001$	5020	1011	158	$P = 0.014$	0.0206	0.0047	158	$P < 0.001$
Cold-water												
C1 (202 mm)	282,303	31,393	128		5023	858	128		0.0179	0.0032	128	
C2 (179 mm)	292,511	46,495	139	$F = 6.441$	5396	957	139	$F = 11.854$	0.0189	0.0044	139	$F = 25.381$
C3 (225 mm)	267,588	81,416	127	$P < 0.001$	5693	1420	127	$P < 0.001$	0.0237	0.0109	127	$P < 0.001$

* Mantle length shown in parentheses.

Table V

Results of Tukey multiple comparison tests on calcium and strontium data for warm- and cold-water statoliths

	Calcium					Strontium					Sr/Ca				
Statolith	C 2	C 3	W 1	W 2	W 3	C 2	C 3	W 1	W 2	W 3	C 2	C 3	W 1	W 2	W 3
Cold-water															
C 1	0.650	0.244	0.237	**0.000**	**0.000**	0.102	**0.000**	0.810	0.054	1.000	0.893	**0.000**	0.180	**0.000**	**0.028**
C 2		**0.003**	**0.003**	**0.000**	**0.000**		0.313	0.798	0.999	0.073		**0.000**	0.793	**0.000**	0.309
C 3			1.000	**0.000**	**0.032**			**0.013**	0.458	**0.000**			**0.001**	0.253	**0.006**
Warm-water															
W 1				**0.000**	**0.043**				0.656	0.799				**0.000**	0.987
W 2					0.068					**0.037**					**0.000**

Note: Results significant at the 5% level are indicated in bold.

The dorsoventral axis of crystallization described earlier may account for the curving axis of higher Sr concentrations that extends into the anterior regions of the lateral dome. Since Ca supply sites are distant from the macula, Ca availability does not become limited as the statolith increases in size, hence the Ca levels are higher in the peripheral area of the lateral dome.

The relevance of these deductions to incremental growth of squid statoliths rests in the importance of strontium. Lipinski (1993, p. 259) suggested that good increment visibility is associated with high Sr concentration in squid statoliths. The Sr distribution patterns described here confirm that concept. The area adjacent and anterior to the cone-shaped intrusion of wing crystals shows the greatest promise for increment enumeration studies, since it is in this region that increments are consistently visible to the margin (Lipinski *et al.,* unpub. data; and see Fig. 3D). This region is the area of the adult statolith that is closest to the cells of the macula, and hence the proposed Sr supply, and shows high Sr contents in all microprobe maps of adult statoliths. Clear increments also occur along a curved axis extending from the nucleus into the anterior regions of the lateral dome; again, this distribution corresponds to the areas of high Sr concentration observed in this study. In contrast, marginal areas of the lateral dome of adult statoliths generally show no increments; these regions correspond to areas of low Sr concentration.

The relationship between Sr distribution patterns and increment visibility can be explained by the results of Mugiya and Satoh (1995), who documented relatively higher Sr concentrations in the discontinuous zones of increments in fish otoliths. Each increment comprises a "light" incremental zone and a "dark" discontinuous zone. Clear increments are a product of clearly defined discontinuous zones, and hence layers of high Sr content.

We can only speculate on the physiological processes linking Sr content to statolith growth, but Hanlon *et al.* (1989) have clearly demonstrated that Sr availability is critical to normal statolith growth. In a number of cephalopod species, a lack of Sr in ambient seawater resulted in either a complete absence of statoliths or the formation of grossly deformed statoliths. Mugiya and Tanaka (1995) indicated that in fish otoliths, strontium may successfully compete with calcium in binding to some kinds of protein. We suggest that a Sr-protein complex stabilizes the aragonite wing crystals in the reverse reactions of deposition and resorption, and that these crystals then serve as a template for the subsequent deposition of other parts of the statolith. We therefore argue that statolith formation is a process triggered, and possibly controlled, by Sr levels in the statocyst that are linked with the protein component. Details of this process, as well as the extent to which it is coupled or modified by other factors (such as pH; Morris, 1988), need to be investigated.

Effects of temperature, sex, and oxytetracycline injection

Statoliths from individuals collected more than 600 km apart in cold (9°C) and warm (18°C) waters showed no major differences in Ca and Sr distribution patterns, indicating that temperature does not influence the basic biomineralization processes occurring in squid statocysts. Sex and maturity also appeared to have no influence on the basic distribution patterns of Sr and Ca. The between-individual variability in Ca and Sr concentrations observed in this study indicates that a larger sample size is required to establish whether temperature, sex, and maturity influence the concentrations of these elements in statoliths.

The data obtained from the 5 OTC-marked statoliths indicated that the incorporation of this compound did not

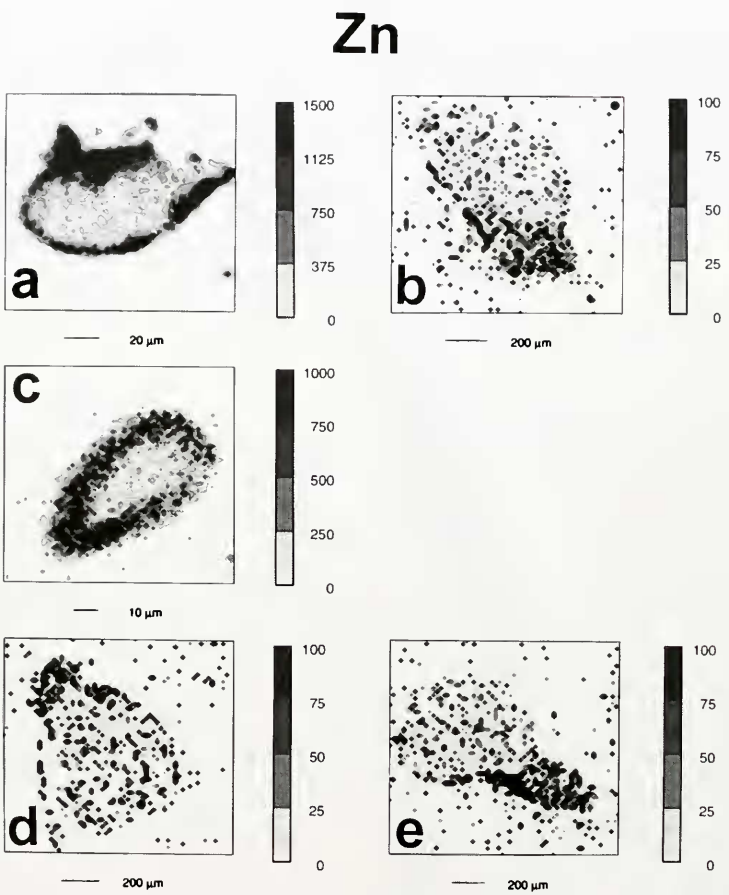

Figure 10. Zinc concentrations (values in ppm) in selected squid statoliths: (a) paralarva; (b) ML = 182 mm, ♀V; (c) paralarva; (d) ML = 214 mm, ♂IIf; (e) ML = 214 mm, ♂II.

have a detectable influence on Ca and Sr levels in the statolith. If any effects did occur, they were on a scale below the resolution limits of the microprobe.

Other elements present

Many different elements have been investigated for various reasons in otoliths, mollusc shells, ostracods, and brachiopods by means of a proton microprobe (Gauldie *et al.,* 1992, 1995; Sie and Thresher, 1992; Coote and Trompetter, 1995; Dai *et al.,* 1995; Nystrom *et al.,* 1995; Bruckschen *et al.,* 1995). The first PIXE results on squid statoliths were reported by Durholtz *et al.* (1995). The present study concentrated on Ca and Sr, but other elements such as Zn, Cu, and Br were also detected and, on the basis of their distribution within the statolith contour, were considered to be genuine parts of the statolith composition. Their concentration was highly variable (*e.g.,* Zn), and they were detected only in certain statoliths. Explanation and description of the presence-absence pat-

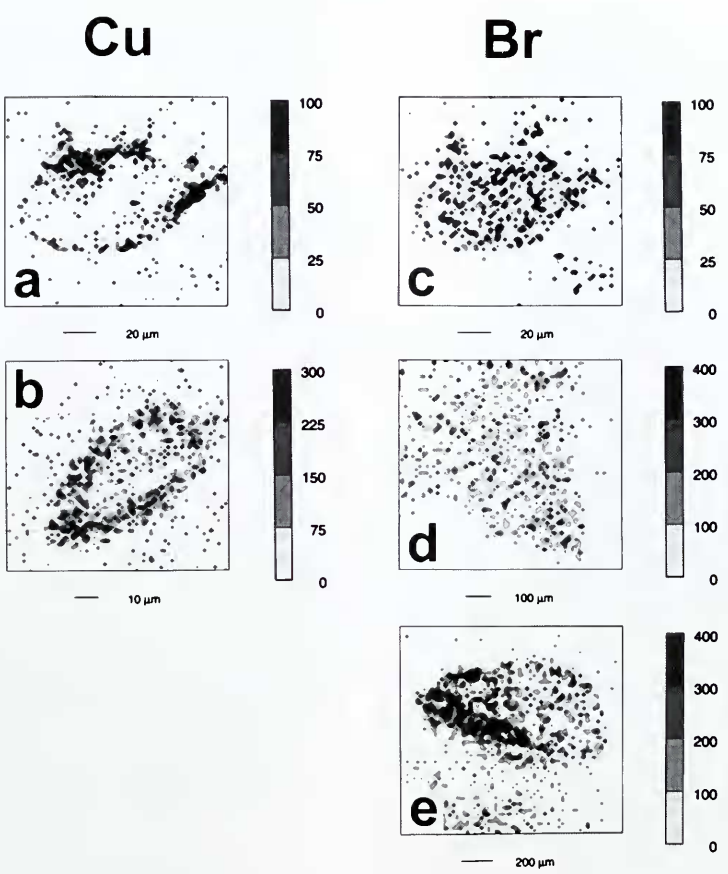

Figure 11. Copper and bromium concentrations (values in ppm) in selected squid statoliths: (a–c) paralarvae; (d) ML = 78 mm, ♂I; (e) ML = 202 mm, ♂II.

terns of these elements must await further investigation. It must also be pointed out that, because of the constraints of the method used, some elements of possible significance (*e.g.,* F; see Coote and Trompetter, 1995) were not investigated at all.

Acknowledgments

The authors are grateful to the staff of Electron Microscopy Unit at University of Cape Town for assistance provided during the course of this study. We also thank Mr. Tony van Dalsen (SFRI) for assistance with the illustrations, and Dr. Rob Tilney for critically reviewing the manuscript.

Literature Cited

Amirikas, R., D. N. Jamieson, and S. P. Dooley. 1993. Measurement of (p,p) elastic cross sections for C, O and Si in the range 1.0–3.5 MeV. *Nucl. Instr. Meth. Phys. Res. B* **77:** 110–116.

Arkhipkin, A. I., V. A. Bizikov, V. V. Krylov, and K. N. Nesis. 1996. Distribution, stock structure, and growth of the squid *Berryteuthis magister* (Berry, 1913) (Cephalopoda, Gonatidae) during summer and fall in the western Bering Sea. *Fish. Bull.* **94:** 1–30.

Bruckschen, P., F. Bruhn, J. Meijer, A. Stephan, and J. Veizer. 1995. Diagenetic alteration of calcitic fossil shells: proton micro-

probe (PIXE) as a trace element tool. *Nucl. Instr. Meth. Phys. Res. B* **104:** 427–431.

Clarke, M. R. 1978. The cephalopod statolith—an introduction to its form. *J. Mar. Biol. Assoc. U.K.* **58:** 701–712.

Coote, G. E., and W. J. Trompetter. 1995. Proton microprobe studies of fluorine distributions in mollusc shells. *Nucl. Instr. Meth. Phys. Res. B* **104:** 333–338.

Dai, Z., C. Ren, Q. Zhao, P. Wang, and F. Yang. 1995. Quantitative micro-PIXE and micro-probe analysis of ostracod shells to reconstruct the paleoenvironment. *Nucl. Instr. Meth. Phys. Res. B* **104:** 619–624.

Doolittle, L. R. 1986. A semiautomatic algorithm for Rutherford backscattering analysis. *Nucl. Instr. Meth. Phys. Res. B* **15:** 227–231.

Durholtz, M. D., M. R. Lipinski, W. J. Przybylowicz, and J. Mesjasz-Przybylowicz. 1995. Structural relations of calcium and strontium in squid statoliths. *Electron Microsc. Soc. South Afr. Proc.* **25:** 74.

Gauldie, R. W., and D. G. A. Nelson. 1990. Interactions between crystal ultrastructure and microincrement layers in fish otoliths. *Comp. Biochem. Physiol. A* **97(4):** 449–459.

Gauldie, R. W., G. C(*sic*). Coote, K. P. Mulligan, and I. F. West. 1992. A chemical probe of the microstructural organization of fish otoliths. *Comp. Biochem. Physiol. A* **102(3):** 533–545.

Gauldie, R. W., I. F. West, and G. E. Coote. 1995. Evaluating otolith age estimates for *Hoplostethus atlanticus* by comparing patterns of checks, cycles in microincrement width, and cycles in strontium and calcium composition. *Bull. Mar. Sci.* **56(1):** 76–102.

Hanlon, R. T., J. P. Bidwell, and R. Tait. 1989. Strontium is required for statolith development and thus normal swimming behaviour of hatchling cephalopods. *J. Exp. Biol.* **141:** 187–195.

Lipinski, M. R. 1981. Statoliths as a possible tool for squid age determination. *Bull. Acad. Pol. Sci. Ser., Sci. Biol.* **28:** 569–582.

Lipinski, M. R. 1986. Methods for the validation of squid age from statoliths. *J. Mar. Biol. Assoc. U. K.* **66:** 505–526.

Lipinski, M. 1991. Scanning electron microscopy (SEM) and chemical treatment. Pp. 97–112 in *Squid Age Determination Using Statoliths,* P. Jereb, S. Ragonese, and S. von Boletzky, eds. NTR-ITPP Special Publication 1, Mazara del Vallo, Italy.

Lipinski, M. R. 1993. The deposition of statoliths: a working hypothesis. Pp. 241–262 in *Recent Advances in Cephalopod Fisheries Biology,* T. Okutani, R. K. O'Dor, and T. Kubodera, eds. Tokai University Press, Tokyo.

Lipinski, M. R., and M. D. Durholtz. 1994. Problems associated with ageing squid from their statoliths: towards a more structured approach. *Antarct. Sci.* **6(2):** 215–222.

Lipinski, M. R., and L. G. Underhill. 1995. Sexual maturation in squid: quantum or continuum? *S. Afr. J. Mar. Sci.* **15:** 207–223.

Lipinski, M., E. Dawe, and V. Natsukari. 1991. Introduction. Pp. 77–81 in *Squid Age Determination Using Statoliths,* P. Jereb, S. Ragonese, and S. von Boletzky, eds. NTR-ITPP Special Publication 1, Mazara del Vallo, Italy.

Lipinski, M. R., M. A. Compagno Roeleveld, and L. G. Underhill. 1993. Comparison of the statoliths of *Todaropsis eblanae* and *Todarodes angolensis* (Cephalopoda: Ommastrephidae) in South African Waters. Pp. 263–273 in *Recent Advances in Cephalopod Fisheries Biology,* T. Okutani, R. K. O'Dor, and T. Kubodera, eds. Tokai University Press, Tokyo.

Lipinski, M. R., W. J. Przybylowicz, M. D. Durholtz, and J. Mesjasz-Przybylowicz. Quantitative micro-PIXE mapping of squid statoliths. *Nucl. Instr. Meth. Phys. Res. B* **212** (in press).

Morris, C. C. 1988. Statolith growth lines and statolith function in the Cephalopoda. Ph.D. Dissertation, University of Cambridge, U. K. 140 pp.

Mugiya, Y., and C. Satoh. 1995. Strontium-calcium ratios change corresponding to microincrements in otoliths of the goldfish *Carassius auratus. Fish. Sci.* **61(2):** 361–362.

Mugiya, Y., and S. Tanaka. 1995. Incorporation of water-borne strontium into otoliths and its turnover in the goldfish *Carassius auratus:* effects of strontium concentrations, temperature, and 17β-estradiol. *Fish. Sci.* **61(1):** 29–35.

Natsukari, Y., H. Mukai, S. Nakahama, and T. Kubodera. 1993. Age and growth estimation of a gonatid squid, *Berryteuthis magister,* based on statolith microstructure (Cephalopoda: Gonatidae). Pp. 351–364 in *Recent Advances in Cephalopod Fisheries Biology,* T. Okutani, R. K. O'Dor, and T. Kubodera, eds. Tokai University Press, Tokyo.

Nyström, J., U. Lindh, E. Dunca, and H. Mutvei. 1995. A study of *M. margaritifera* shells from the River Pauliströmsän, S. Sweden. *Nucl. Instr. Meth. Phys. Res. B* **104:** 612–618.

Prozesky, V. M., W. J. Przybylowicz, E. van Achterbergh, C. L. Churms, C. A. Pineda, K. A. Springhorn, J. V. Pilcher, C. G. Ryan, J. Kritzinger, H. Schmitt and T. Swart. 1995. The NAC nuclear microprobe facility. *Nucl. Instr. Meth. Phys. Res. B* **104:** 36–42.

Research Systems Inc. 1993. *Interactive Data Language, User's Manual.* Boulder, CO. USA.

Romanek, C. S., and R. W. Gauldie. 1996. A predictive model of otolith growth based on the chemistry of fish endolymph. *Comp. Biochem. Physiol. A* **114(1):** 71–79.

Ryan, C. G., and D. N. Jamieson. 1993. Dynamic Analysis: on-line quantitative PIXE microanalysis and its use in overlap-resolved elemental mapping. *Nucl. Instr. Meth. Phys. Res. B* **77:** 203–214.

Ryan, C. G., D. R. Cousens, S. H. Sie, W. L. Griffin, G. F. Suter, and E. Clayton. 1990. Quantitative PIXE microanalysis of geological material using the CSIRO proton microprobe. *Nucl. Instr. Meth. Phys. Res. B* **47:** 55–71.

Ryan, C. G., D. N. Jamieson, C. L. Churms, and J. V. Pilcher. 1995. A new method for on-line true elemental imaging using PIXE and the proton microprobe. *Nucl. Instr. Meth. Phys. Res. B* **104:** 157–165.

Sie, S. H., and R. E. Thresher. 1992. Micro-PIXE analysis of fish otoliths: methodology and evaluation of first results for stock discrimination. *Int. J. PIXE* **2(3):** 357–379.

Tapper, U. A. S., W. R. McMurray, G. F. Ackermann, C. Churms, G. de Villiers, D. Fourie, P. J. Groenewald, J. Kritzinger, C. A. Pineda, J. Pilcher, H. Schmitt, K. Springhorn, and T. Swart. 1993. High-brightness proton beams at the NAC nuclear microprobe by acceleration of H_2 ions. *Nucl. Instr. Meth. Phys. Res. B* **77:** 17–24.

Van Achterbergh, E., C. G. Ryan, J. J. Gurney, and A. P. le Roux. 1995. PIXE profiling, imaging and analysis using the NAC proton microprobe: unraveling mantle eclogites. *Nucl. Instr. Meth. Phys. Res. B* **104:** 415–426.

Villanueva, R. 1992. Interannual growth differences in the oceanic squid *Todarodes angolensis* Adam in the northern Benguela upwelling system, based on statolith growth increment analysis. *J. Exp. Mar. Biol. Ecol.* **159:** 157–177.